# Non-reciprocal interactions in the XY Model

Author: David Mazzanti Tarancón

*Master en Física dels Sistemes Complexos i Biofísica.*
*Facultat de Física, Universitat de Barcelona, Martí i Franquès 1, 08028 Barcelona, Spain*

Advisor: Demian Levis Sotomayor

**Abstract:** This work focuses on the investigation of non-reciprocal interactions in the XY Model using the Kuramoto model of synchronization in the overdamped limit. Initially, we provide partial results of the reciprocal XY Model by examining the spatial correlation function and the transition temperature. Through a comparison of simulation and theoretical results, we gain insights into the critical behavior of the model. To extend the analysis, we introduce non-reciprocal interactions using the Kuramoto model in the overdamped regime, which offers a nonlinear mathematical framework for understanding the dynamics of the system. This is particularly relevant as the reciprocal XY Model lacks a Hamiltonian description. By incorporating non-reciprocal interactions, we observe that the system does not undergo a topological phase transition. Instead, a dynamic analysis reveals, under certain initial distribution and conditions, the emergence of waves and their characteristic propagation. We explore these phenomena in both one-dimensional and two-dimensional scenarios, demonstrating that the waves propagate with a linear velocity and exhibit a linear dispersion relation.

## I. INTRODUCTION

In the realm of statistical mechanics, the 2D XY Model has captivated researchers as a fundamental model for studying critical phenomena, ranging from phase transitions to magnetism [1]. This model was studied by J.M. Kosterlitz and D.J. Thouless in the early 1970s and describes the behavior of a two-dimensional array of spins that interact with each other through a nearest-neighbor coupling [2].

This model has proven to be an important tool in order to understand the collective behaviour of systems that exhibit a continuous symmetry. Its simplicity and tractability have made it an ideal platform to investigate different phenomena, including topological defects and the Berezinskii–Kosterlitz–Thouless (BKT) transition. These phenomena are distinct from the conventional symmetry-breaking phase transition observed in other interaction models such as the Ising model. This type of phase transition drives the system from a quasi-long-range order (QLRO) phase to a disordered phase. BKT transitions have been found in different contexts like boson gases [3], liquid crystals [4] and superconductors [5].

Most of the investigations related to the XY Model have been focused on reciprocal interactions, where the coupling between neighbour spins is symmetric and bidirectional. However, in recent years, a growing interest has emerged in exploring systems with non-reciprocal interactions where the coupling term is no longer symmetric. Non-reciprocity induces new features in the system's dynamics that are absent in the conventional XY Model.

Non-reciprocal interactions break the action-reaction principle. This is a direct consequence of the absence of a straightforward Hamiltonian formulation and the inability to define an energy for the system. In reciprocal systems, the Hamiltonian governs the dynamics of the model and allows the understanding of the system's behaviour. However, non-reciprocal interactions typically require a different description that goes beyond the conventional Hamiltonian framework [6] [7].

One prominent model that can be employed to study the dynamics of non-reciprocal interactions is the Kuramoto model [8]. Originally introduced to describe the synchronization of coupled oscillators, this model has a wide range of applications in different fields, including physics, biology and social dynamics. In the context of the XY Model, the Kuramoto model provides a new framework to model the interactions between spins considering both their inherent dynamics and the influence of non-reciprocal couplings. Furthermore, by considering the spins as oscillators and incorporating the non-reciprocal nature of the interactions into the Kuramoto model, we can effectively capture the emergence of collective behavior and synchronization transitions.

Non-reciprocal interactions have already been studied in the XY Model. For instance, the introduction of vision cone interactions has lead to the apparition of new phenomena such as the emergence of long-range order and the propagation of large domains within the system [6]. In this scenario, spins exclusively interact with particles confined within a specific vision angle, resulting in unique dynamical and collective behaviors. Additionally, the Kuramoto model of synchronization has been successfully employed to incorporate non-reciprocal interactions. For instance, this model has been used to explore the nature of non-reciprocal interactions among particles that can freely rotate and move throughout

the system. This has revealed distinct phase transitions and properties not observed in the reciprocal case [7]. These findings shows the impact of non-reciprocity on the dynamics and collective behavior of the XY Model, offering new ways for understanding complex systems and critical phenomena.

In this work, we will study how non-reciprocal interactions are induced in the XY Model by means of the Kuramoto model in the overdamped regime. The first section provides a description of the XY Model, highlighting its fundamental properties and phenomena. We provide a mathematical formulation of the model and the emergence of topological defects within the system, inducing a BKT transition. Simulation results are presented, showing the emergence of vortex-antivortex pairs and the transition from QLRO phase to a disordered phase as temperature increases.

In section III, we give a description of the Kuramoto model and its relation with the XY Model. The section highlights its relevance in capturing the dynamics of the model. In section IV, we introduce non-reciprocal interactions in the XY Model, defining the dynamics with the Kuramoto model. We provide an initial insight of how non-reciprocity affects the system under specific initial conditions.

In section V, we emphasize the limitations of studying static variables when capturing the complexity of non-reciprocal systems, demonstrating the necessity of exploring dynamical variables, which are introduced in section VI. In this section, the exploration of dynamical properties reveals the emergence of new patterns and behaviors never reported before in the context we are analyzing, unveiling new wave propagation properties characteristic of the system.

## II. XY MODEL

The XY Model is a 2D interacting lattice model where the spins are represented as a unit vector pointing in a plane. Each spin has only two components and it can be parameterized as

$$\mathbf{S}_i = \begin{pmatrix} cos(\theta_i) \\ sin(\theta_i) \end{pmatrix} , \qquad (1)$$

where $\theta_i$ is the angle with respect to an arbitrary axis of the plane. The Hamiltonian of the system, in absence of an external magnetic field, is given by

$$H = -J \sum_{\langle i,j \rangle} \mathbf{S_i} \cdot \mathbf{S_j} = -J \sum_{\langle i,j \rangle} cos(\theta_i - \theta_j) , \qquad (2)$$

where $J$ is the coupling constant that determines the strength of the interaction between spins. Here $\langle i, j \rangle$ denotes summation over all nearest neighbour sites in the lattice.

The XY Model has a $O(2)$ continuous symmetry. The Hamiltonian defined in Eq. 2 is invariant under global rotations, $\theta_i \rightarrow \theta_i + \theta_0$. The ground state at zero temperature corresponds to fully aligned states, where all the spins in the plane point towards the same direction with $\theta_i = \theta$ for all $i$. Since all the directions are equivalent, the system exhibits an infinite degeneracy in its ground states. This allows for a global rotation without any energy cost. As a consequence, the free energy of the system has an infinite number of minima and any excitation of the ground state leading to a global rotation leaves the free energy invariant. These excitations, known as Goldstone or soft modes, are characteristic of systems with continuous symmetry. The presence of these modes suppress the possibility of having long-range order at any finite temperature. A visual representation of the potential is shown in Fig. 1.
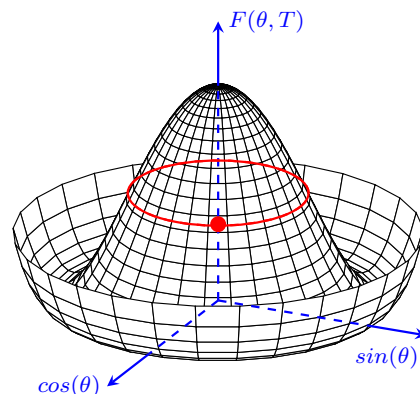


Figure 1: Free energy's potential shape associated to the XY Model. The red line represents an equipotential contour where a particle (red dot) can move freely without any energy cost. The system exhibits an infinite degeneracy at each potential value, allowing all the spins to orient in any direction within the plane.

### A. Spin-wave approximation

The XY Model, initially formulated in two dimensions, can be extended to any higher dimension $D$. For instance, consider a D-dimensional lattice governed by the Hamiltonian defined in Eq. 2, where the summation term still accounts for nearest neighbors. As we increase the dimension of the system, the number of neighbors increases accordingly. At low temperatures, we can assume that the angles between adjacent spins are small enough, $|\theta_i - \theta_j| << 1$. Therefore, the cosine term in the Hamiltonian can be approximated by expanding it to second

order, leading to

$$H \approx -J \sum_{\langle i,j \rangle} \left[ 1 - \frac{1}{2}(\theta_i - \theta_j)^2 \right] \ . \tag{3}$$

Eq. 3 can be conveniently expressed in terms of a vector **r**, representing the positions of the spins on the lattice with respect to an arbitrary origin in the coordinate system. Additionally, we can also introduce another vector **a**, which points to any direction within the plane with magnitude $a$, representing the lattice spacing. With these definitions, the Hamiltonian can be written as

$$H \approx E_0 + \frac{J}{2} \sum_{i,\mathbf{a}} (\theta(\mathbf{r_i}) - \theta(\mathbf{r_i} - \mathbf{a}))^2 \ . \tag{4}$$

This formulation allows us to describe the system in terms of the angle's difference between neighbor spins, considering their positions and the lattice spacing. Here $E_0$ denotes the energy of the completely aligned ground state of $N$ spins, $E_0 = -\frac{JNz}{2}$, with $z$ the coordination number of the lattice. If $\theta(\mathbf{r})$ is a slowly varying function of $\mathbf{r}$, we can approximate the finite difference by a derivative $\theta(\mathbf{r}-\mathbf{a}) - \theta(\mathbf{r}) \approx a\partial_{\mathbf{x}}\theta(\mathbf{r})$ since $a << |\mathbf{r}|$. Thus, if the system is large enough, the sum over lattice sites can be approximated to an integral $(\sum_{\langle \mathbf{r} \rangle} \rightarrow \frac{zd}{a^d} \int d^d r)$. Therefore, the Hamiltonian can be written as

$$H \approx E_0 + \frac{Jzd}{2a^{d-2}} \int d^d\mathbf{r} \left[ \nabla\theta(\mathbf{r}) \right]^2 \ , \tag{5}$$

where we can define $\rho_s = \frac{Ja^{2-D}z}{2D}$ as the generalized stiffness. From the expression given by Eq. 5, we can study the order parameter, or magnetization, of the system in the low-temperature phase for any dimension. In the continuous limit, we can define this magnitude as follows

$$\langle S_x \rangle = \langle cos(\theta(\mathbf{r})) \rangle = \frac{1}{Z} \int \mathcal{D}[\theta] \ e^{-\beta H} \cdot Re\left( e^{i\theta(\mathbf{r})} \right) \tag{6}$$

where $\mathcal{D}[\theta]$ represents the integration measure over all possible configurations of the field $\theta(\mathbf{r})$. This equation can be expressed in the Fourier space as

$$\langle S_x \rangle = \frac{1}{Z} \int_{-\infty}^{\infty} \prod_{|q|<\lambda} d\theta_q \ exp\left( -\frac{\beta}{2}\rho_s \sum_q q^2 |\theta_q|^2 - i\sum_q \theta_q \right) \ . \tag{7}$$

Since Eq. 7 is a gaussian type integral, its result is

$$\langle S_x \rangle = e^{-W} \ ; \ W = \frac{k_B T \lambda^{D-2}}{2\rho_s(D-2)} \ . \tag{8}$$

For more calculus details, see, for instance, [9]. The $W$ factor is known as the Debye-Waller factor and diverges for $D = 2$ (XY Model). This leads to a magnetisation value of $\langle S_x \rangle = 0$ for all temperatures except $T = 0$. This implies that, for any non-zero temperature, the system cannot establish long-range order. Consequently, the system lacks a low-temperature ordered phase and cannot undergo a symmetry-breaking phase transition in two

dimensions. This result is a consequence of the Mermin-Wagner theorem, which states that systems with short-range interactions in dimensions below a critical value cannot exhibit spontaneous broken symmetry at a finite temperature [10]. It is important to note, however, that this result is specific to the particular order parameter considered. This does not exclude that other order parameters can take non-zero value at any non-vanishing temperatures.

### B. Topological defects

From Eq. 5, we can derive the field configurations that correspond to local minima of the energy $H$ by solving the extremal condition:

$$\frac{\delta H}{\delta\theta(\mathbf{r})} = 0 \Rightarrow \nabla^2\theta(\mathbf{r}) = 0 \ . \tag{9}$$

This result corresponds to the Laplace equation, and one of the solutions is the ground state where $\theta(\mathbf{r})$ is constant and all spins point in the same direction. However, a second type of solutions are also allowed, known as vortices in the plane. These vortices can be obtained by imposing a set of boundary conditions on the circulation integral of $\theta(\mathbf{r})$:

- For all closed curves that enclose the center position of a vortex

$$\oint \nabla\theta(\mathbf{r}) \cdot d\mathbf{l} = 2\pi q \ , \tag{10}$$

where $q$ is the *charge* of the vortex. This condition imposes a singularity on the plane.

- For all paths that does not enclose the vortex

$$\oint \nabla\theta(\mathbf{r}) \cdot d\mathbf{l} = 0 \ . \tag{11}$$

The vortices in the plane represent topological defects, which are localized regions of the system where the spins deviate from the ground state configuration. These defects corresponds to local minima of the potential energy and the system cannot be smoothly transformed into a fully aligned ground state. In other words, there is no spatial transformation such as

$$\mathbf{s}(\mathbf{r}) \rightarrow R(\mathbf{r})\mathbf{s}(\mathbf{r}) \ , \tag{12}$$

with a continuous rotation matrix $R(\mathbf{r})$ that can deform a configuration with a topological defect into a fully aligned ground state configuration.

In the 2D XY Model, these topological defects manifest as vortices. Vortices can have attractive or repulsive behavior depending on their charge value, denoted as $q$. The presence of vortices breaks the uniform order of the system. The inability to remove vortices without the creation of additional vortices is a consequence of the topological nature of the defects within the system.

### C. Topological phase transition

The creation of a single vortex has associated an energy cost. This can can be computed from Eq. 5, depending on the value of $\nabla\theta$. By imposing the boundary condition defined in Eq. 10 and considering the spherical symmetry of the system, we can derive this relationship. The circulation integral around the vortex can be expressed as

$$2\pi q = \oint \nabla\theta(\mathbf{r}) \cdot d\mathbf{l} = 2\pi r \left|\nabla\theta\right| \Rightarrow \left|\nabla\theta\right| = \frac{q}{r} \ , \qquad (13)$$

where $r$ is the radial distance from the vortex center. This equation shows that the magnitude of the gradient of $\theta$ is inversely proportional to the radial distance and directly proportional to the charge of the vortex.

Substituting the expression for $\left|\nabla\theta\right|$ into the Hamiltonian given by Eq. 5, we can determine the energy associated with a single vortex creations, which can be expressed as

$$E \equiv E_{vortex} - E_0 = \pi q^2 J \ ln\left(\frac{L}{a}\right) \ , \qquad (14)$$

where $L$ is the linear size of the system and $a$ the distance between spins. From this equation, we observe that the energy cost of a single vortex diverges logarithmically in the infinite size limit. As the linear size $L$ of the system increases, the energy required to create a vortex also increases. This logarithmic divergence indicates that it becomes increasingly energetically unfavorable to introduce vortices in larger systems.

The presence of topological defects can induce a phase transition. To verify this, we can analyze the free energy difference between configurations with and without vortices. The configurational entropy, which represents the number of different lattices sites where the vortex can be located at, is given by

$$S = k_B \ ln\left(\frac{L^2}{a^2}\right) = 2k_B \ ln\left(\frac{L}{a}\right) \ . \qquad (15)$$

Here, $k_B$ is the Boltzmann constant, $L$ is the linear size of the system, and $a$ is the distance between neighboring spins. Considering the temperature $T$, the free energy associated with the creation of a vortex can be expressed as

$$F = E - TS = (\pi J - 2k_B T) \ ln\left(\frac{L}{a}\right) \ . \qquad (16)$$

From Eq. 16, we can infer that if $k_B T > \frac{\pi J}{2}$, the system can lower its free energy by creating vortices. Below the critical temperature, isolated vortices cannot exist, but above this temperature, they can be present in the system. At the critical temperature, the system undergoes a phase transition characterized by the spontaneous

creation of single vortices. This transition is known as Berezinskii–Kosterlitz–Thouless (BKT) phase transition.

Although the energy associated to a vortex diverges as $ln(L)$, the energy of a bound pair of vortex-antivortex does not diverge because the total vorticity of the pair cancels out at a distances larger than the distance between the vortices. Consequently, below the BKT transition temperature $T_{BKT}$, vortices can exist in the system but only in the form of bound pairs. This behavior can be observed in Fig. 2, which shows the final configuration of a simulation of the XY Model with a system size of $L = 100$. As we increase the system size of the lattice, we expect to find more pairs of vortices around the system.
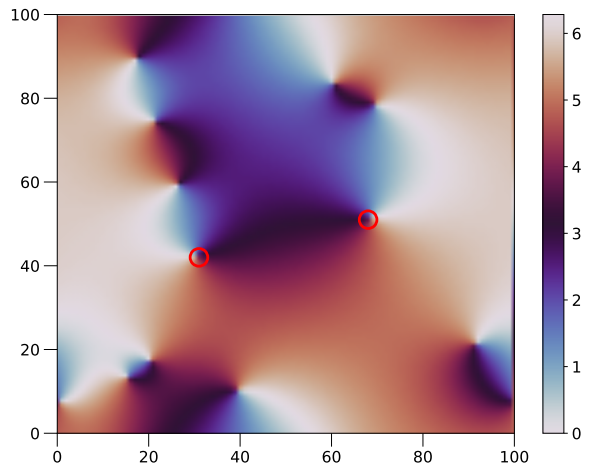


Figure 2: Final configuration of a simulation of the XY Model with periodic boundary vortices at a temperature $T = 0$. Particles were initially pointing to different random directions. Vortices are denoted by red circles.

Furthermore, the BKT transition is characterized by the unbinding of these vortex-antivortex pairs. Above the critical temperature $T_{BKT}$, the vortices pairs dissociate, leading to the spontaneous creation of individual vortices. This behavior can be observed by comparing the system snapshots at two different temperatures, as shown in Fig. 3.

In the XY Model, the transition temperature is estimated to be at

$$T_C \equiv T_{BKT} \sim 0.893 \ , \qquad (17)$$

in units of $J/k_B$ (from now on, all temperature values will be given in these units). This result is different from the approximation $T_{BKT} = \frac{\pi}{2}$ as computed numerically [11]. It is worth noting that below the critical temperature, thermal fluctuations can lead to the creation and annihilation of vortex-antivortex pairs before the system reaches equilibrium.
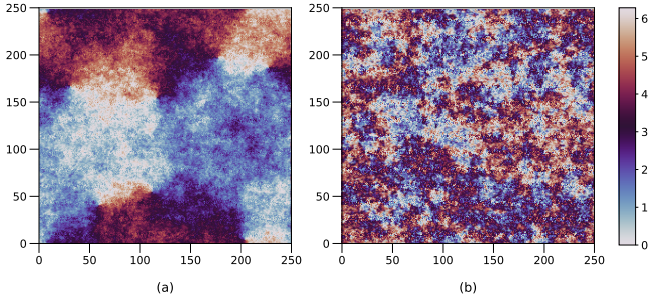
Figure 3: Final configurations of the XY Model simulations with PBC and a system size of $L = 250$. (a) Temperature below the critical temperature ($T_{BKT} = 0.2$) exhibiting quasi-long-range order (QLRO). (b) Temperature above the critical temperature ($T_{BKT} = 1.0$) displaying a disordered phase.

### D. Correlation function

The BKT transition in the XY Model differs from the typical symmetry-breaking phase transitions observed in models like the 2D Ising Model. In the BKT transition, the order parameter of the system does not change significantly above and below the critical temperature. Instead, the transition is characterized by a change from a state of quasi long-range order (QLRO) to a disordered phase. In a QLRO state, the relevant correlation function exhibits an algebraic decay. This is in contrast to the exponential decay observed in systems with short-range or long-range order.

This difference in the correlation function behavior is a key distinction between topological phase transitions (TPT) and symmetry-breaking phase transitions (SBPT). In SBPT, the power-law decay is observed only at the critical temperature, while above and below this temperature, the correlation function decays exponentially with a characteristic correlation length $\xi$. In contrast, for TPT, the algebraic behavior of the correlation function persists at all temperatures below the critical point. As the temperature exceeds the critical point, thermal fluctuations become dominant, causing the correlation function to decay exponentially with an associated correlation length.

To analyze the correlation function, we will consider a two dimensional lattice neglecting any vortex fluctuation in the system. The correlation funcion $G(\mathbf{r}) \equiv \langle \mathbf{S}(\mathbf{r})\mathbf{S}(0) \rangle$ can be computed as

$$\langle \mathbf{S}(\mathbf{r})\mathbf{S}(0) \rangle = \langle cos(\theta(\mathbf{r})\theta(0)) \equiv Re \left\langle e^{i(\theta(\mathbf{r}) - \theta(0))} \right\rangle . \quad (18)$$

This can be further expressed as an integral over all possible field configurations in the canonical ensemble,

$$\langle \mathbf{S}(\mathbf{r})\mathbf{S}(0) \rangle = \frac{1}{Z} \int D[\theta] \, e^{-\beta H} \cdot Re \left( e^{i(\theta(\mathbf{r}) - \theta(0))} \right) , \quad (19)$$

where $Z$ denotes the partition function of the system. Using the Hamiltonian defined in the spin-wave approximation, Eq. 19 can be expressed in the Fourier space as

$$G(r) = \frac{1}{Z} \int_{-\infty}^{\infty} \prod_{|q|<\lambda} d\theta_q$$

$$exp\left(-\frac{\beta}{2}\rho_s \sum_q q^2|\theta_q|^2 - i\sum_q \theta_q + i\sum_q \theta_q e^{iqr}\right) . \quad (20)$$

To analyze the decay of correlations, we define a function $g(r)$ such that $G(r) = e^{-g(r)}$. This function $g(r)$ can be expressed as:

$$g(r) = \frac{k_B T}{\rho_s} \int \frac{d^D q}{(2\pi)^D} \frac{1 - e^{-i\mathbf{q}\cdot\mathbf{r}}}{q^2} . \quad (21)$$

Here, $d^D q = q^{D-1} dq d\Omega$ accounts for the integration measure in $D$ dimensions, and $d\Omega$ represents the solid angle element. By performing the integration, we can approximate the integral as:

$$g(r) \sim \int_{\pi/L}^{\pi/a} dq \frac{q^{D-1}}{q^2} \sim \int_{\pi/L}^{\pi/a} \frac{dq}{q^{3-D}} \quad (22)$$

For calculus details, see, for example, appendix C of [12]. In the case of the XY Model in two dimensions ($D = 2$), the function $g(r)$ exhibits a logarithmic divergence, specifically as $g(r) \sim \ln\left(\frac{r}{L}\right)$. For $T < T_{BKT}$, the correlation function follows a power-law decay,

$$G(r) \sim \left(\frac{r}{L}\right)^{-\eta(T)} \quad ; \quad \eta(T) = \frac{k_B T}{2\pi\rho_s} . \quad (23)$$

As mentioned earlier in this subsection, above the critical temperature the correlation function decays as an exponential. Simulations results are shown in Fig. 4.

From this plot, we can see that the behavior of $G(r)$ changes qualitatively as the system crosses the critical temperature .This transition in the correlation function can be attributed to the presence of vortices in the system. Below the critical temperature $T_c$, the system forms bound pairs of vortices, which locally breaks the ordering. Beyond a certain distance from the paired vortices, the spins align in the same direction. This establishment of quasi-long-range order reflects in the correlation function.

Above $T_c$, the system becomes completely disordered, and thermal fluctuations lead to the creation and annihilation of vortices. The unbinding of vortex pairs generates short-range correlations, resulting in an exponential decay of $G(r)$. This behavior is indicative of the absence of long-range order and the prevalence of thermal fluctuations.
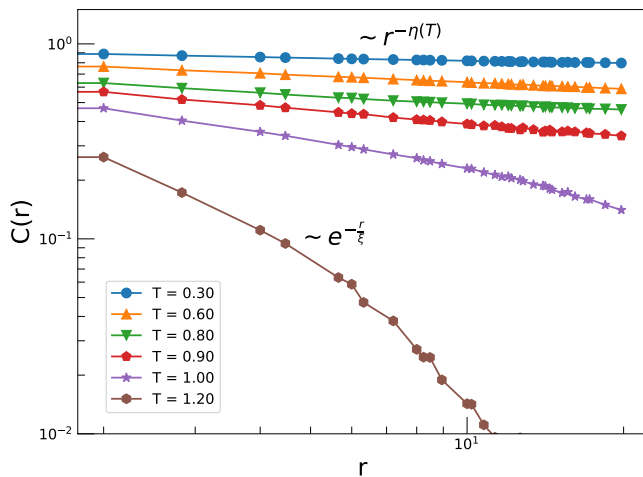
Figure 4: Spatial correlation function evolution for different temperatures in log-log scale for a system size $L = 100x100$. Below the critical temperature, the correlations decay as a power-law defined by Eq. 23 that changes with temperature. Above the critical temperature, the correlations decay exponentially due to the disordered phase of the system.

It is important to note that the power-law and exponential behaviors of the correlation function described previously apply only at the stationary state of the system. To verify that the system has equilibrated, we can measure the space-time correlation function at different times, defined as

$$G(r,t) = \langle \mathbf{S}(\mathbf{r},t)\mathbf{S}(0,t) \rangle \ . \qquad (24)$$

The space-time correlation function provides information into the evolution of correlations over time and helps us to understand how the system reaches its equilibrium state. Fig. 5 illustrates the temporal correlation function and its behavior as the system evolves.

From Fig. 5, we can see that as the system evolves, the correlation function reaches an asymptotic behavior where the correlation functions overlap with each other. This indicates that the system has reached equilibrium. However, it is important to note that the simulated value $\eta_{\text{sim}}(T)$ obtained from the fitting procedure deviates from the analytical value $\eta(T)$. the discrepancy between both values is attributed to finite-size effects in the simulation. While the analytical results are derived under the assumption of an infinitely large system in the thermodynamic limit ($N \rightarrow \infty$), simulations are typically performed on systems of finite size.

### III.  KURAMOTO MODEL

The dynamics of the XY Model can be described by the Kuramoto model, a nonlinear mathematical model used to study synchronization phenomena. The Kuramoto
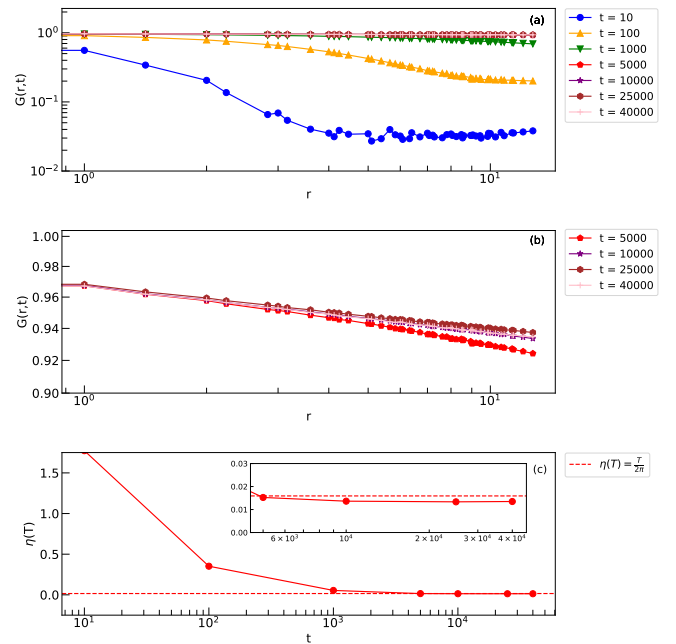


Figure 5: Simulation results for a system size of $L = 100$ at $T = 0.1$ with $J = 1.0$. (a) Temporal correlation function for different times of the simulation. (b) Temporal correlation function for times near the equilibrium state. (c) Evolution of the exponent $\eta(T)$ for each time fitting all the points data to a power law $r^{-\eta(T)}$. Dashed line represents the exact value in units of $J/k_B$. Inset plot are the values associated to plot (b).

model provides a framework for understanding the behavior of a large ensemble of coupled oscillators, where each oscillator is characterized by its natural frequency $\omega_i$. The dynamics of the model are governed by the following equation for each oscillator,

$$\dot{\theta}_i = \omega_i + \sum_{j=1}^{K} J_{ij} sin(\theta_i - \theta_j), \ i = 1, ..., N \ , \qquad (25)$$

where each one tends to run independently at its own frequency $\omega_i$, while the coupling term $\sum_{j=1}^{K} J_{ij} \sin(\theta_i - \theta_j)$ tends to synchronize it with the other oscillators in the system. This model has been successfully applied in a wide range of applications, from neural networks to oscillations of chemical reactions [13].

The Kuramoto model is closely linked to the dynamics of the XY Model, as both involve spins that can freely rotate and interact with their neighbors to achieve synchronization. The equations of motion for the Kuramoto model in the overdamped regime are given by a set of coupled Langevin equations [14]:

$$\frac{d\theta_i}{dt} = \omega_i + J \sum_{\langle i,j \rangle} sin(\theta_i - \theta_j) + \sqrt{\Gamma}\eta_i(t) \qquad (26)$$

where $\eta_i(t)$ is a Gaussian white noise representing ther-

mal fluctuations. The thermal noise is characterized by the following properties

$$\langle \eta_i(t) \rangle = 0 \; ; \; \langle \eta_i(t)\eta_j(t') \rangle = \Gamma \delta_{i,j} \delta(t-t') \;, \quad (27)$$

Here, $\langle . \rangle$ denotes averaging over noise realizations and $\Gamma$ represents the strength of the Gaussian noise. According to the Fluctuation-Dissipation Theorem, $\Gamma$ is related to the temperature as $\Gamma = 2k_B T$. In reduced units, the overdamped dynamics of the model can be written as

$$\frac{d\theta_i}{d\tilde{t}} = \tilde{\omega}_i + \sum_{\langle i,j \rangle} sin(\theta_i - \theta_j) + \tilde{g}\tilde{\eta}_i(\tilde{t}) \quad (28)$$

where

$$\tilde{t} \equiv Jt \; ; \; \tilde{\omega}_i \equiv \frac{\omega_i}{J} \; ; \; \tilde{\eta}_i \equiv \frac{\eta_i(t)}{J} \; ; \; \tilde{g} \equiv \sqrt{\frac{\Gamma}{J}} \; .$$

where $\tilde{t} \equiv Jt$, $\tilde{\omega}_i \equiv \frac{\omega_i}{J}$, $\tilde{\eta}_i \equiv \frac{\eta_i(t)}{J}$, and $\tilde{g} \equiv \sqrt{\frac{\Gamma}{J}}$. Therefore, the Kuramoto dynamics can be understood as the overdamped dynamics of an XY Model with nearest neighbor coupling, influenced by a heat reservoir that introduces thermal fluctuations. The parameter $\tilde{\omega}_i$ represents an external driving amplitude present in the system. When $\tilde{\omega}_i = 0$, the model corresponds to the XY Model in the presence of thermal fluctuations.

In our simulations, we focus on the overdamped dynamics equation defined in Eq. 28 with $\tilde{\omega}_i = 0$. This corresponds to the overdamped limit of the Kuramoto model with identical oscillators under the influence of Gaussian white noise. By neglecting the external driving force $\tilde{\omega}_i$, we will only investigate the non-reciprocity introduced by the interaction between different species. This limit corresponds to Kuramoto model with identical oscillators in presence of a gaussian white noise. The dynamics of the system are reduced to a classical statistical system in contact with a heat bath, governed by equilibrium statistical mechanics.

## IV. NON-RECIPROCAL XY MODEL

Non-reciprocal interactions are of great interest as they often arise in natural systems, particularly when the system is in a non-equilibrium medium. However, these interactions are challenging to modelize because they lack a Hamiltonian description that can fully capture the system's properties. Unlike systems governed by reciprocal interactions, non-reciprocity breaks Newton's third law, and the establishment of an energy scale becomes problematic, even in the ground state. Furthermore, the absence of reciprocal interactions has significant implications for the long-term behavior of the system, since it lacks of a well-defined equilibrium state to which it can converge.

To introduce non-reciprocal interactions in the XY Model, we modify the spin interactions in the system. In

this case, we consider a square lattice of size $L \times L$ composed of spins belonging to two different species, labeled as $A$ and $B$. These spins can rotate in the plane. In the general scenario, the system will include interaction between different species and between the same species, as well as thermal fluctuations. As a result, the dynamical equations for each spin can be written as follows:

$$\dot{\theta}_i = \sum_{k,\tilde{k} \in \{A,B\}} \sum_{\langle i,j \rangle} J_{k,\tilde{k}} \; sin(\theta_i - \theta_j) + \sqrt{\Gamma}\eta_i(t) \;, \quad (29)$$

where $J_{k,\tilde{k}}$ represents the interaction strength between spins of species $k$ and $\tilde{k}$ (the only possible combinations are $J_{AA}$, $J_{AB}$, $J_{BA}$, $J_{BB}$). Notice that intraspecies interactions are always reciprocal while interspecies interactions are not.

The study of non-reciprocal interactions will be under the an specific initial configuration. To ensure that all interactions within the system are non-reciprocal, we arrange the spins of different species alternately on the lattice assuming a temperature of $T = 0$ to eliminate any thermal fluctuations. Specifically, we assign a positive value to the interaction between species $A$ and $B$, denoted as $J_{AB} > 0$, and a negative value between species $B$ and $A$, denoted as $J_{BA} < 0$. An illustration of this configuration is provided in Fig. 6.
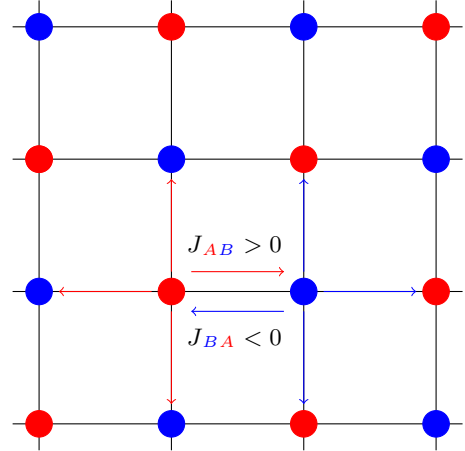


Figure 6: Representation of a $LxL$ square lattice composed by two species, A (red) and B (blue), that interact with their nearest neighbours. A species interact ferromagnetically with B (denoted with red arrows) and B species interact antiferromagnetically with A (denoted with blue arrows).

The dynamical equations for each spin reduces as follows:

$$\dot{\theta}_i = J_{AB} \sum_{\sum_{j \in n_i}} sin(\theta_i - \theta_j) + J_{BA} \sum_{\sum_{j \in n_i}} sin(\theta_i - \theta_j) \;. \quad (30)$$
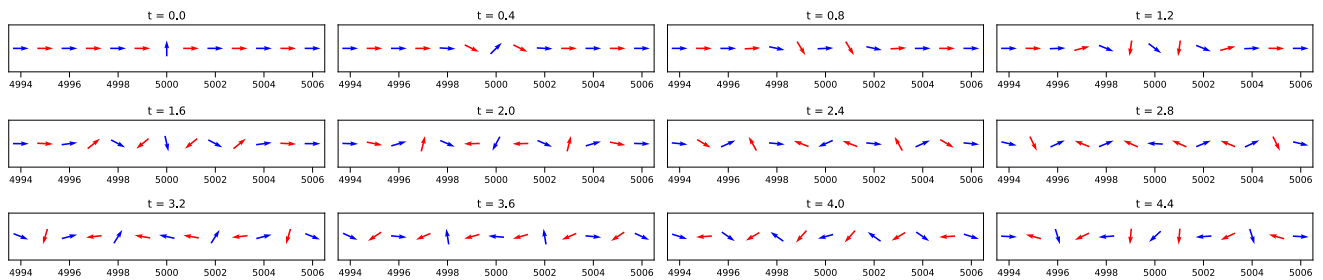
Figure 7: Time evolution of a 1D chain system consisting of $N = 10000$ spins (snapshots only taken for the central spins), divided into two species, $A$ (red) and $B$ (blue). The initial state of the system is set to all spins with an angle of $\theta_i = 0$, except for the central spin which has $\theta = \pi/2$. This setup allows to observe the propagation of interactions throughout the chain, as spins actively compete to establish an order. Over time, local groups of spins align or antialign with each other. However, this local ordering gradually breaks down as interactions continue to influence the system.

In this context, the system is expected to undergo an active competition between the two species in order to establish an order throughout the lattice. The $A$ particles will attempt to align with the $B$ particles due to their ferromagnetic interaction. Conversely, the $B$ particles will want to be antialigned with the $A$ particles due to their antiferromagnetic interaction. This competition will disrupt the QLRO behavior that we observed below the critical temperature of the XY Model. While nearby spins of the same species may align in the same direction due to their shared neighbors and similar interactions, the system's ordering will break as soon as there is no connection between these spins.

In order to understand the effect of non-reciprocal interactions on the system, consider a one-dimensional chain consisting of two different species, $A$ and $B$, which are arranged alternately along the entire chain. Initially, all spins point in the same direction, except for the central spin of the system, which is displaced by an angle of $\pi/2$ with respect to the overall direction. This angular displacement ensures that the interaction between neighboring spins is maximized right from the start. A time evolution of the system can be observed in Fig. 7.

As time progresses, the system undergoes a dynamic where the red spins attempt to align with the blue spins if the angle difference between them is non-zero. Since the system is maintained at a temperature of $T = 0$, no spin fluctuations are expected, and the time evolution is governed by the Kuramoto equations. As we can see at $t = 0.4$ in Fig. 7, we observe that the central blue spin tries to align with its neighboring red spins, while red ones actively avoid this alignment. Consequently, their neighboring particles prevent this alignment. This initiates a chain reaction that propagates throughout the system, triggered by the relaxation of the angle constraint.

It is important to note that the propagation is symmetric with respect the central blue spin due to

the dynamics of the Kuramoto model. The model does not consider the specific location of the angular displacement but focuses on the difference in angles between the interacting spins. Furthermore, if we observe the figure at $t = 3.6$, red particles point to the same direction, indicating local ordering. This occurs due to the disordering exhibited by the blue spins. In the subsequent time step, red particles maintain their alignment while blue ones begin to align with their respective neighbors. Consequently, this disrupts the local ordering of the red spin, causing each spin to assume a new direction based on the angle difference with its neighbors.

Eventually, at $t = 4.4$, the blue particles locally align, while the red ones enter in a disordered phase. This behavior persists as the interaction propagates throughout the system. Localized spins of one species align in a period of time, while the particles of the other species maintain a relatively disordered phase. After that period, the local ordering between species is exchanged.

Introducing temperature to the system will disrupt its deterministic behavior. The propagation of the initial perturbation will gradually decrease as it propagates along the chain. The particles will interact with neighbors whose angles have been influenced by thermal fluctuations. The speed at which the propagation disappears depends on the temperature of the system. Higher temperatures will lead to a faster disappearance of the propagation.

## V. STATIC ANALYSIS OF THE NON-RECIPROCAL XY MODEL

Just like in the XY Model, the presence of a topological phase transition in the system can be determined by examining the behavior of the spatial correlation function with increasing temperature. Similarly, we can extend our investigation to understand how the

ordering of the lattice evolves in the equilibrium state when non-reciprocal interactions are present throughout the system. To explore this, we consider a 2D square lattice model as depicted in Fig. 6. By studying the correlations between spins of the same kind and averaging over multiple realizations, we can obtain insights into the behavior of the system. The resulting correlation function is depicted in Fig. 8.
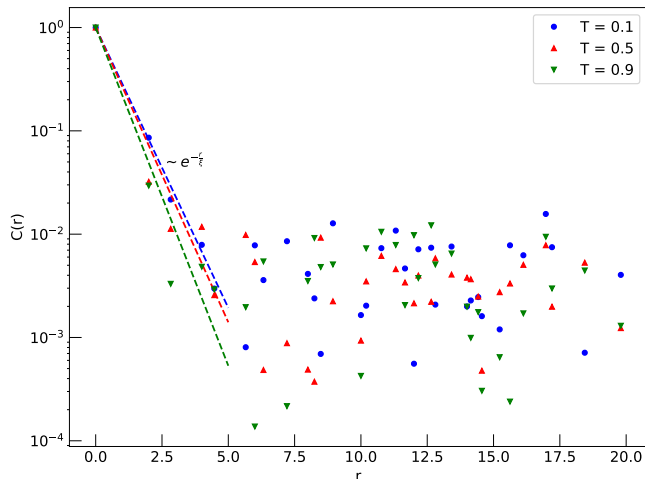


Figure 8: Spatial correlation function evolution for different temperatures in log-log scale for a system size $L = 100x100$ with non-reciprocal interactions over the system, set at $J_{AB} = 1.0$ and $J_{BA} = -1.0$. Results are averaged over different realizations with different initial configuration. Correlation values are only computed with species of the same kind.

In contrast to the reciprocal case, the correlation function in the presence of non-reciprocal interactions displays an exponential decay for all temperature values, unlike the power-law behavior observed below the critical temperature of approximately $T \sim 0.9$ found in the reciprocal case. Consequently, the system does not undergo a BKT transition when non-reciprocal interactions are introduced. As the correlation function decays exponentially faster at any temperature, the system remains in a disordered phase indefinitely. This behavior holds true not only for a completely antiferromagnetic interaction, but for any interaction satisfying $0 \leq J_{BA} < -1.0$ when a fixed value of $J_{AB} = 1$ is maintained.

The correlation length, represented by $\xi$, increases as $J_{AB}$ approaches to $-1.0$, indicating that correlations become unbound at shorter distances. For interaction values within the range $1.0 > J_{BA} > 0.0$, correlations between spins of the same kind are still present, but the correlation function decays exponentially. Consequently, no BKT transition occurs in the system. This absence of bound vortices can be attributed to the active competition between the species, causing the system

to continually change the direction of the spins locally. The instability experienced by the system prevents the formation of vortex pairs, as observed in the 1D chain model.

From these results we can see that, in the non-reciprocal XY Model, static measures are proven to be inadequate in capturing the essential characteristics of the system. Unlike in the reciprocal case, where static measures such as the spatial correlation function and the order parameter are important indicators of the system's behavior, their application in the non-reciprocal setting does not yield to meaningful results. As we have seen, this limitation arises due to the dynamic and competing nature of the non-reciprocal interactions. The active competition between species disrupts the establishment of long-range order at any temperature and introduces significant fluctuations in the system. As a result, static measures fail to capture the collective behavior that arises from the interplay between non-reciprocal interactions and thermal fluctuations.

## VI. DYNAMIC ANALYSIS OF THE NON-RECIPROCAL XY MODEL

The system's behavior of the non-reciprocal XY Model can be studied by looking at the dynamical properties. Unlike the reciprocal case, non-reciprocal interactions introduce a dynamic and competitive nature that needs a shift towards a dynamical analysis. By investigating the temporal evolution of the system under specific conditions using the Kuramoto model, we can capture the intricate dynamics that arise from the competition between species and the impact of thermal fluctuations. These dynamical measurements can provide an understanding of the emergent phenomena governed by the system dynamics behavior. This is in contrast with the reciprocal XY Model, where dynamical properties have limited relevance since the system's behavior can be captured by static measures. Thus, the exploration of dynamical properties using the Kuramoto model presents an opportunity to study the complex dynamics of the system.

As discussed in the previous sections, the Kuramoto model of synchronization is a valuable tool for understanding the dynamics of couples oscillators, assuming that the presence of only a minimal amount of noise does not disrupt the overall behavior. Applying this concept to the XY Model, we can understand the spins within the system as oscillators that continuously transits between different directions. This analogy allows us to explore the dynamic nature of the XY Model, particularly at zero temperature, where the absence of thermal fluctuations enables us to see the spins as deterministic oscillators rather than random variables.

### A.   1D analysis

The dynamical properties of the model can be studied under certain conditions. For instance, we can consider the 1D configuration illustrated in Fig. 7 where, initially, all spins are aligned in a particular direction except for the central spin, which is flipped by an angle $\theta_i = \pi/2$. Temperature is set to $T = 0$ in order to avoid any thermal fluctuation. This specific configurations leads to a *propagation* of the initial perturbation within the chain, propagating in both the right and left directions. This interaction propagates analogously as a *wave* across the chain. This wave-like propagation can be observed by computing the dot product between neighboring spins, quantifying the directionality between adjacent spins. This dot product is defined as

$$\mathbf{S_i} \cdot \mathbf{S_{i+1}} = cos(\theta_i - \theta_{i+1}) \ . \tag{31}$$

where $\mathbf{S_i}$ and $\mathbf{S_{i+1}}$ is denotes the spin direction located at positions $i$ and $i + 1$ of the chain, respectively. By examining the numerical results depicted in Fig. 9, we can clearly observe the propagation of the initial perturbation in the form of distinct wave-like structures. In fact, these are travelling waves and are characteristic of nonlinear systems. They arise due to the non-reciprocity of the interactions and the Kuramoto dynamics. The travelling shape of these waves remains consistent over time and they travel at a constant velocity. It is important to highlight that the waves are generated by the initial configuration of the system, but the periodic waves they produce eventually dissipate. Furthermore, when these waves reach the boundaries of the system, they collide with other traveling waves resulting from the PBC of the simulation. These collisions leads to the dissipation of the wave propagation and the dynamics inherent to the model.

To determine the velocity of the periodic waves produced by the system, we can track their positions at different time intervals. By monitoring the position of the initially generated node as it propagates through the chain (both at right and left from the flipped spin located at the center of the chain), we can extract the wave's velocity. Since all waves in the system travel at the same constant velocity, the speed of the first node is equivalent to the subsequent waves formed. Furthermore, these waves are non-dissipative as their shape remains unchanged over time, exhibiting stability and consistency in structure. This property can already be seen in Fig. 9. In this figure, we illustrate the dot product defined by Eq. 31 for a sequence of spins in the 1D chain. The dot product is computed for each spin with its immediate right neighbor, indicating whether the particles are aligned ($\mathbf{S}i \cdot \mathbf{S}i + 1 > 0.5$) or antialigned ($\mathbf{S}i \cdot \mathbf{S}i + 1 < -0.5$). Intermediate values indicate that the spins are close to a perpendicular position.
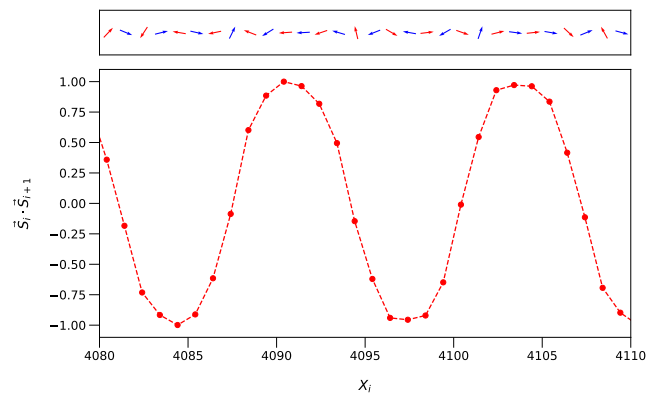


Figure 9: The top panel illustrates a region of the configuration of a 1D chain consisting of $N = 10000$ particles. Interaction strengths are set to $J_{AB} = 1.0$ and $J_{BA} = -1.0$ with a system's temperature of $T = 0$. The snapshot was taken after $t = 2000$ time steps. The dot product values with neighboring particles are plotted as a function of the spin position $X_i$. The oscillatory shape is not preserved throughout the entire chain due to the non-equilibrium nature of the interactions, eventually leading to a transition into a disordered phase.

The position of a node at different times is depicted in Fig. 10. As can be seen from this figure, the wave position shows a clearly linear relationship with time, indicating a constant velocity of wave propagation.
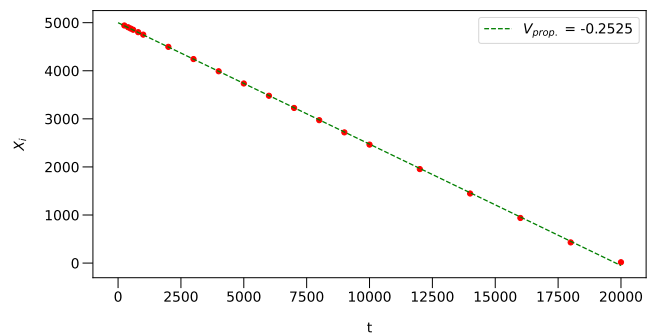


Figure 10: Positions of travelling waves $X_i$ at different time $t$ values are shown in the figure. The relationship between position and time is analyzed linearly, determining the velocity of the wave as the slope of the linear fitting, with $V_{prop.} = -0.2525$. The simulations were performed on a 1D chain comprising $10,000$ particles, with the interaction strengths set to $J_{AB} = 1.0$ and $J_{BA} = -1.0$.

The propagation velocity of the wave depends on the intensity of the interaction. By fixing $J_{AB} = 1.0$, we can observe distinct behaviors based on the choice of $J_{BA}$. When $J_{BA} = -1.0$, representing a fully antiferromagnetic interaction, the travelling wave achieves the maximum velocity. Conversely, with $J_{BA} = 0.0$, where there is no interaction between the central spin and its neighbors, there is no wave propagation. These varia-

tions in the interaction strength reveal the sensitivity of the wave motion to the underlying non-reciprocal interactions in the system.

We can further investigate the wave propagation in the system by examining its dispersion relation, which characterizes the relationship between the wavelength and temporal frequency of the waves. To determine the wavelength, we analyze the distances between peaks in Fig. 9, representing the periodic production of waves before they become disordered. By averaging these distances, we can calculate the corresponding wave number. Additionally, we study the temporal evolution of a wave by observing how the dot product of its position changes over time. The periodic behavior of the waves allows us to identify the period by measuring the distances between successive peak waves. From this, we can calculate the frequency. By computing the quotient $\frac{\omega}{k}$, we can examine whether the relationship between $k$ and $\omega$ follows a linear pattern. The dispersion relation behavior is shown in Fig. 12. The obtained results for the wavenumber and the period are presented in Fig. 11.

The velocities are in good agreement for both analysis. These results are important because they prove that the dispersion relation is linear, indicating that both the phase velocity and the group velocity are the same.

This study can also be extended for positive values of $J_{BA}$ when fixing $J_{AB} = 1.0$. However, the results obtained in this case are not particularly significant. When both interactions are ferromagnetic, the system quickly reaches an equilibrium configuration where all the spins align in the same direction. Consequently, there is no wave propagation along the chain, and the system maintains its uniform structure through all the chain. As we increase the value of $J_{BA}$, the speed at which the system reaches this configuration becomes faster, causing all the spins to align in a shorter period of time. As a result, waves are not produced within the system.

A similar phenomenon occurs when temperature is introduced. The presence of thermal fluctuations disrupts the consistent shape of any wave that arises, preventing the propagation of coherent waves along the chain. With the introduction of fluctuations, each spin in the system undergoes continuous changes at each time step. This can be visualized as the generation of individual wave propagation by each spin, which subsequently collide with waves generated by neighboring spins. As a result, the system becomes fully disordered for any noticeable temperature, where the effects of thermal fluctuations become increasingly significant over time. For extremely low temperature values with $T \to 0$, the system behaves as if it were unaffected by those fluctuations.

The wave propagation interaction extend beyond only one spin that is initially flipped by an angle of $\theta_i = \pi/2$.
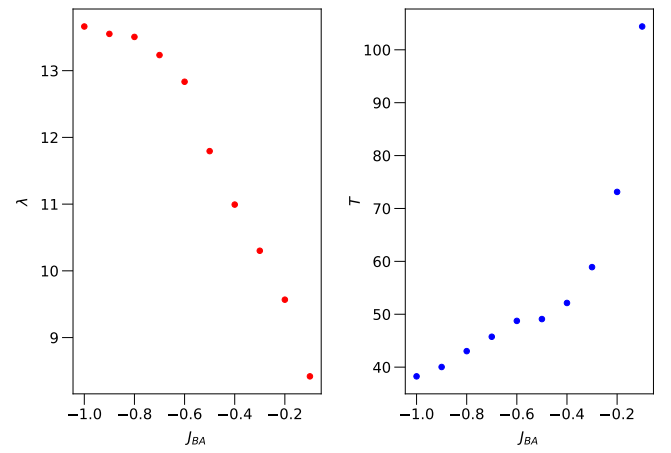


Figure 11: Wavelength (left) and period (right) results for different values of the interaction term $J_{BA}$ (with fixed $J_{AB} = 1.0$) at $T = 0.0$. As the interaction term $J_{BA}$ is reduced, the wavelength of the propagating waves decreases, while the time period between consecutive peaks for a fixed spin increases. This phenomenon results in a decrease in the propagation velocity, as depicted in Fig. 12. Notice that for $J_{BA} = 0.0$ results are not plotted since there is no wave propagation.
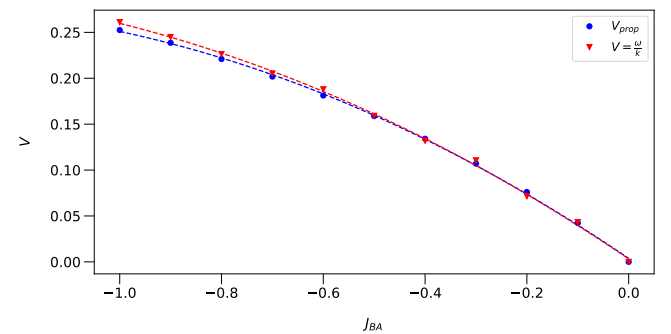


Figure 12: The figure depicts the propagation velocities of travelling waves generated by the initial configuration of the system. The blue curve represents the velocities obtained through linear fitting of positions at different times, as illustrated in Fig. 10, for different $J_{BA}$ interaction terms while keeping $J_{AB} = 1.0$ fixed. The red curve represents the quotient of the wavenumber $k$ and the angular frequency $\omega$. Both measurements exhibit a good fit, the last one indicating that the system follows a linear dispersion relation.

Any region within the system where the boundaries exhibit an angle difference compared to their neighboring spins will exhibit the same properties. When considering a region where spins have an angle difference $\Delta\theta_i = \pi/2$ with spins outside this region, waves are produced at the boundaries and travel along the chain in both directions. The propagation is not limited to the direction where spins initially point in a different direction; it also extends in the opposite direction where the spins are initially aligned. This behavior arises from the inherent dynamic properties of spins that present an angle difference

with some of their neighbors, as they induce a movement in the next time step that alters their orientations and interacts with the initially aligned spin.

### B. 2D analysis

The analysis done in the previous subsection can be extended to two dimensions. Wave properties of the system can be studied by considering different boundaries and initial configurations at zero temperature. However, compared to the 1D case, the increased number of interactions in 2D systems leads to distinc propagation characteristics. Simply examining the dot product between neighboring spins becomes challenging for computing wave propagation, as each spin interacts with four nearest neighbors. Consequently, the effect of interactions between two specific spins is significantly reduced due to the presence of other neighboring spins. Nevertheless, wave propagation phenomena still manifest in the system.

A different approach for analyzing wave propagation interactions in the system involves examining the chirality between plaquettes in the square lattice. In this context, a plaquette can be defined as a square-shaped arrangement of four spins, with one spin located a each corner of the square. The total chirality of the plaquette ($C$) can be determined computing the cross product between neighboring spins. A visual representation of this concept is depicted in Fig. 13.



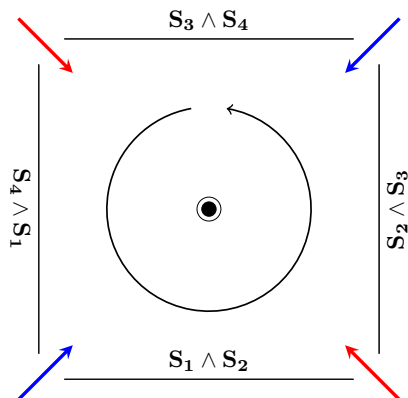Figure 13: Plaque composed by 4 spins in a square lattice. The central value of the circulation is computed from Eq. 32.

The chirality of the lattice is defined as the sum of the all the cross product between neighbour spins,

$$C = \sum_{i=1}^{3} \mathbf{S_i} \wedge \mathbf{S_{i+1}} + \mathbf{S_4} \wedge \mathbf{S_1} \ . \tag{32}$$

By examining the chirality within plaquettes, we can infer the propagation of the nodes through the system.

In contrast to the 1D case, particle interactions in the 2D lattice will be transmitted through four neighboring spins instead of two. By looking at the cross product between adjacent spins, we can determine their relative orientations. Analyzing all the interactions within a plaquette of spins provides information their rotation in the plane and, consequently, their alignment within the system.

We can study wave propagation in a similar manner to the 1D case. Initially, we arrange the spins of different species alternately on the lattice with a temperature of $T = 0$, as shown in Fig. 6. All spins, except for the central one, are initially aligned in the same direction. The central spin is flipped by an angle of $\pi/2$ with respect to the other spins, inducing a propagation of the initial perturbation throughout the system. To visualize this propagation, we compute the chirality of each plaquette in the system, each one formed by four adjacent spins. Spins that have not been affected by the initial perturbation will remain aligned, with no net chirality value. For spins that have been influenced by the perturbation, a net chirality value will be observed.

A snapshot of the system can be visualized at Fig. 14. As we can see from the figure, waves are produced again (in space and time) by the initial situation of the system. However, in this case, the wave propagation does not occur throughout the entire lattice but rather along specific contours, denoted in a red ellipse in the figure. This behavior is a consequence of the system's geometry and the initial configuration.
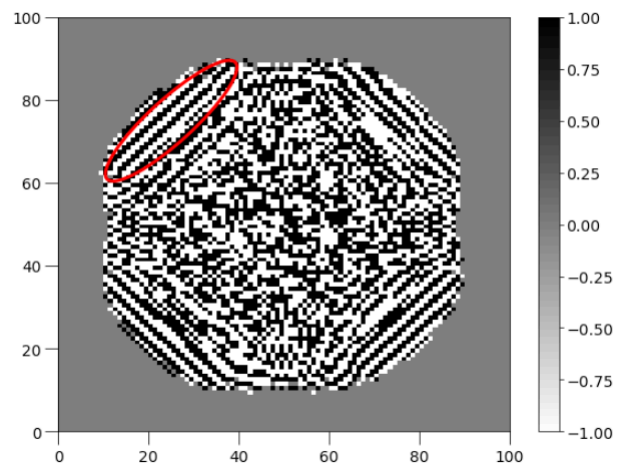


Figure 14: Normalized chirality values for each plaquette in the lattice are presented in this figure. The sign of the computed values is shown, with black nodes indicating a clockwise chirality ($= 1.00$), white nodes denoting counterclockwise chirality ($= -1.00$), and grey nodes representing no net chirality. Red ellipse denotes a region where regular waves are propagating.

Performing a similar analysis as in the 1D chain, we can determine the velocity of the wave propagation. In this case, we measure the distance between the center of the circle and a traveling wave located at the contour of the circle. For instance, we consider a wave positioned within the red ellipse shown in Fig. 14, measuring the distance at different time points. Since waves propagate in various directions, we average the distances over different directions at each time point, obtaining a more accurate estimation of the position of the traveling wave relative to the center of the circle. Using the averaged results, we perform a linear fitting of the wave's positions at different times, similar to the analysis seen in Fig. 10. This allows to determine the velocity of the traveling wave in the 2D lattice.

Furthermore, we can investigate whether the dispersion relation remains linear in this case. Similar to the 1D chain, we compute the wavelength for different negative values of the $J_{BA}$ interaction, keeping $J_{AB} = 1.0$ fixed. The wavelength is determined by measuring the distance between consecutive peaks for the chirality values of each plaquette, averaging the results over different directions to obtain an accurate value. To determine the frequency, we measure the distance between peaks for the chirality values of a fixed spin of the lattice over consecutive times. All the results are presented in Fig. 15.
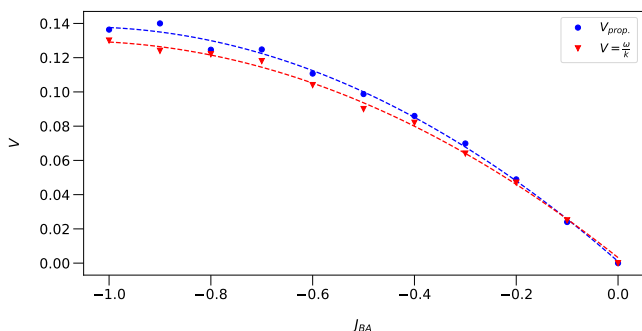


Figure 15: Propagation velocities of travelling waves generated by the initial configuration are depicted in the figure. The blue curve represents the velocities obtained through linear fitting of positions of the wave at different times for different $J_{BA}$ interactions. The red curve represents the quotient of the wavenumber $k$ and the frequency $\omega$. The shape of the curve are similar to the 1D chain observed in Fig. 12, but the velocities are smaller.

From these results, we observe that the linear dispersion relation remains valid even in the 2D case, as evidenced by the agreement between the quotient value and the computed wave propagation velocity. This suggests that the addition of an extra dimension does not alter the fundamental nature of wave propagation in the system, but rather affects its velocity. Comparing the fitting results for both the 1D and 2D cases, we

find that waves propagate at a slower rate in the 2D system. This can be attributed to the increased number of interactions in the 2D system, since it doubles the number of interactions for each spin compared to the 1D case. Consequently, it becomes more challenging for the system to propagate these interactions efficiently.

In contrast, when considering positive values of $J_{BA}$ while fixing $J_{AB} = 1.0$, the interactions between different species become ferromagnetic, resulting in the absence of wave propagation in the system. Instead, the system will reach an equilibrium state where all particles are aligned in the same direction. Furthermore, the introduction of thermal fluctuations in the system disrupts the wave propagation of interactions, as spins begin to point in random directions due to thermal disorder.

## VII. CONCLUSIONS

Non-reciprocal interactions in the XY Model introduce dynamical features that are absent in the reciprocal case. The action-reaction principle breaks when different interacting species are introduced, challenging the traditional Hamiltonian formalism. As a consequence, alternative dynamical models need to be employed to capture the system's dynamics accurately. The Kuramoto model of synchronization offers a viable solution by modelling each spin as an oscillator, describing the dynamics using the Langevin overdamped dynamics framework. This approach enables a comprehensive understanding of the system's behavior under non-reciprocal interactions. The introduction of this model in the context of our research leads to novel findings in wave propagation that have not been reported before, indicating unique founds into the dynamics of the system.

The introduction of non-reciprocal interactions disrupts the apparition of the phase transition typically observed in the XY Model. In the reciprocal case, the XY Model undergoes a topological phase transition associated to the unbinding of topological defects, such as vortices. However, in the non-reciprocal framework, the system does not longer preserve this transition. Consequently, the correlation function maintains the exponential behavior seen in the disordered phase. This makes the system hard to be analyzed by looking only at static variables.

By examining the dynamic properties of the system, new phenomena never reported before is unveiled. Specifically, under certain initial conditions, the system exhibits the propagation of interactions in the form of waves that propagates through the system keeping its shape. These wave-like structures can be studied by analyzing the dot product between adjacent spins in a 1D chain or by considering the chirality between plaquettes in the 2D case. However, the apparition of

waves only happens when particles interact distinctly between species. For instance, when species $A$ interacts ferromagnetically with $B$ spins, and $B$ particles interact antiferromagnetically with $A$, the conditions for wave propagation are met. The introduction of thermal fluctuations, disrupts the wave propagation phenomenon, preventing the formation of coherent waves in the system.

When introducing two distinct species, namely $A$ and $B$, into the system with ferromagnetic and antiferromagnetic interspecies interactions, respectively, the resulting interaction waves exhibit a linear dispersion relation in both 1D and 2D configurations. This indicates that the phase and group velocities of the waves are equal. However, it is important to note that the velocities differ when comparing the same interaction conditions in different dimensions. Specifically, in a 1D chain, the wave propagation velocity is faster compared to a 2D system. In a 1D chain, each spin only needs to consider its alignment with adjacent spins, simplifying the competition between neighboring particles. In the 2D scenario, the interactions between spins is extended to 4 neighboring spins. This makes it more challenging for the initial perturbation of the system to propagate through the lattice, resulting in a lower wave propagation velocity compared to the 1D case. This indicates that the presence of additional neighboring spins to interact with introduces more complex dynamics and constraints on the alignment of spins.

Wave propagation in the non-reciprocal XY Model occurs under specific conditions. The occurrence of wave-like propagations is maximized when spins of different species are arranged alternately in the lattice. This configuration ensures that all particles only interact with spins of a different kind. In contrast, in a random initial configuration, the study of wave-like propagations becomes more challenging due to the possibility of intraspecies interactions occurring in the system. Additionally, the lattice arrangement plays an important role in the wave propagation characteristics of the system. Further investigations are needed to analyze wave-propagation type interactions in different lattice structures, such as the triangular lattice one, to determine if similar phenomena are observed in those systems.

### VIII. ACKNOWLEDGMENTS

[1] N. Goldenfeld, "Lectures on phase transitions and the renormalization group", Addison-Wesley, 1992.

[2] J. M. Kosterlitz and D. J. Thouless, "Ordering, metastability and phase transitions in two-dimensional systems", J. Phys. C, vol. 6, pp. 1181-1203, 1973.

[3] Z. Hadzibabic, P. Krüger, M. Cheneau, B. Battelier, and J. Dalibard, "Berezinskii–Kosterlitz–Thouless crossover in a trapped atomic gas", Nature, vol. 441, pp. 1118–1121, 2006.

[4] S. Singh, "Phase transitions in liquid crystals" Phys. Rev. Lett. vol. 324, pp. 107-108, 2000.

[5] A. F. Hebard and A. T. Fiory, "Evidence for the Kosterlitz-Thouless Transition in Thin Superconducting Aluminum Films", Phys. Rev. Lett. vol. 44, pp. 291-295, 1980.

[6] S. A. M. Loos, S. H. L. Klapp, and T. Martynec, "Long-range Order and Directional Defect Propagation in the Nonreciprocal XY Model with Vision Cone Interactions", Phys. Rev. Lett., vol. 130, 198301, 2022.

[7] M. Fruchart, R. Hanai, P. B. Littlewood, and V. Vitelli, "Non-reciprocal phase transitions", Nature, vol. 592, pp. 363-369, 2021.

[8] S. H. Strogatz, "From Kuramoto to Crawford: exploring the onset of synchronization in populations of coupled oscillators", Physica D: Nonlinear Phenomena, vol. 143, no. 1-4, pp. 1-20, 2000.

[9] H. J. Jensen, "The Kosterlitz-Thouless Transition", Imperial College, available at: `https://www.imperial.ac.uk/quantum-physics/materials/jensen/xy_notes.pdf`

[10] N. D. Mermin and H. Wagner, "Absence of ferromagnetism or antiferromagnetism in one- or two-dimensional isotropic Heisenberg models", Phys. Rev. Lett., vol. 17, 1133, 1966.

[11] Y.-D. Hsieh, Y.-J. Kao, and A. W. Sandvik, "Finite-size scaling method for the Berezinskii-Kosterlitz-Thouless transition", Journal of Statistical Mechanics: Theory and Experiment, 2013.

[12] L. F. Cugliandolo, "Notes on Advanced Statistical Physics: Phase Transitions", Université Pierre et Marie Curie – Paris VI. Laboratoire de Physique Théorique et Hautes Energies, 2018.

[13] J. A. Acebrón, L. L. Bonilla, C. J. Pérez Vicente, F. Ritort, and R. Spigler, "The kuramoto model: A simple paradigm for synchronization phenomena", Reviews of Modern Physics, vol. 77, no. 1, pp. 137, 2005.

[14] Y. Rouzaire, D. Levis "Dynamics of topological defectsin the noisy Kuramoto model in two dimensions", Front. Phys., vol. 10, 976515, 2022.